

IGen: Scalable Data Generation for Robot Learning from Open-World Images

Chenghao Gu^{1*} Haolan Kang^{2*} Junchao Lin^{3*} Jinghe Wang¹ Duo Wu¹
 Shuzhao Xie¹ Fanding Huang¹ Junchen Ge¹ Ziyang Gong⁴ Letian Li¹
 Hongying Zheng⁵ Changwei Lv⁵ Zhi Wang^{1,†}

¹Tsinghua University

²HKU ³Beijing University of Chemical Technology

⁴Shanghai Jiao Tong University ⁵Shenzhen University of Information Technology

<https://chenghaogu.github.io/IGen/>

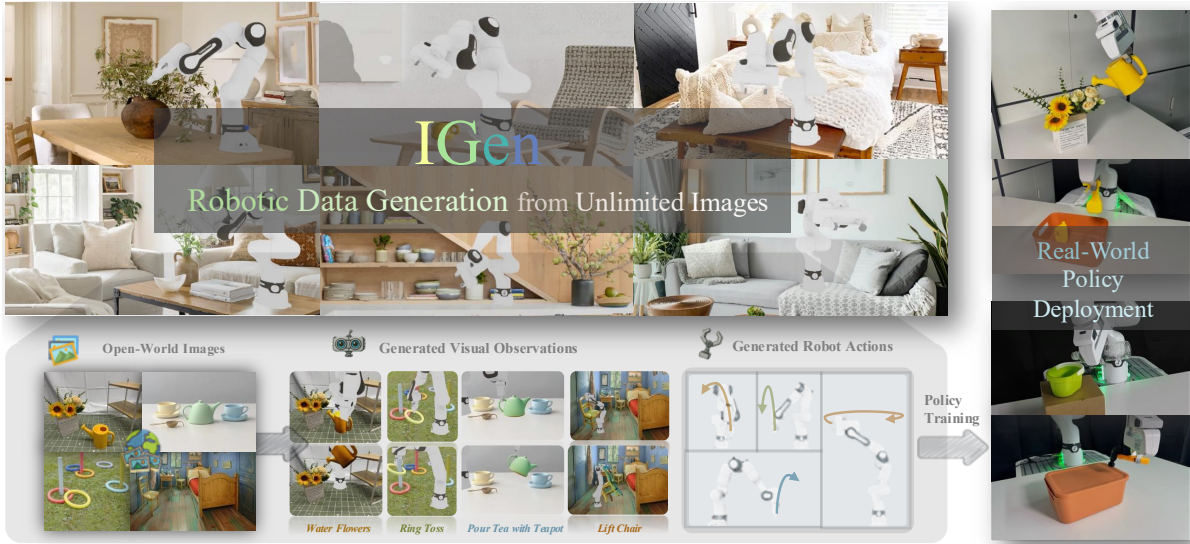


Figure 1. We propose **IGen**, a data generation framework that converts open-world images into grounded visuomotor data, enabling scalable data synthesis for robot learning. From a single image, IGen generates large-scale realistic observations and reliable actions. The policies trained solely on IGen-generated data can effectively generalize to real-world scenes and successfully perform manipulation tasks.

Abstract

The rise of generalist robotic policies has created an exponential demand for large-scale training data. However, on-robot data collection is labor-intensive and often limited to specific environments. In contrast, open-world images capture a vast diversity of real-world scenes that naturally align with robotic manipulation tasks, offering a promising avenue for low-cost, large-scale robot data acquisition. Despite this potential, the lack of associated robot actions hinders the practical use of open-world images for robot learning, leaving this rich visual resource largely unexploited. To bridge this gap, we propose **IGen**, a framework that scalably generates realistic visual observations and executable actions

from open-world images. *IGen* first converts unstructured 2D pixels into structured 3D scene representations suitable for scene understanding and manipulation. It then leverages the reasoning capabilities of vision-language models to transform scene-specific task instructions into high-level plans and generate low-level actions as $SE(3)$ end-effector pose sequences. From these poses, it synthesizes dynamic scene evolution and renders temporally coherent visual observations. Experiments validate the high quality of visuomotor data generated by *IGen*, and show that policies trained solely on *IGen*-synthesized data achieve performance comparable to those trained on real-world data. This highlights the potential of *IGen* to support scalable data generation from open-world images for generalist robotic policy training.

* Equal contribution. † Corresponding author.

1. Introduction

Visuomotor policy learning [4, 5, 11, 33, 68] has shown great promise in enabling robots to perform open-world manipulation, yet it typically requires large-scale paired visual-action data for effective learning. Unfortunately, collecting such data on real robots is labor-intensive and often limited to specific environments. The high cost and environment-specific nature of robotic data collection remain a fundamental bottleneck to the generalization of visuomotor policies across diverse real-world scenarios [46].

In contrast to on-robot data collection, open-world images can be acquired at extremely low cost and encompass a vast diversity of scenarios that naturally align with real-world robotic tasks. Harnessing such rich visual resources offers a promising path toward building scalable, general-purpose robotic policies [37, 73]. Indeed, the remarkable success of large vision-language models (VLMs) [1, 3, 44] has demonstrated that open-world images provide a powerful foundation for training capable, generalist perception systems. However, robotic policy learning imposes unique demands: it requires not only semantically meaningful visual inputs but also physically grounded, executable action sequences [11, 19, 75]. This mismatch prevents the effective utilization of open-world images for robot learning.

To address the complementary limitations of open-world images and robot-collected data, a growing line of work seeks to derive robot-relevant action representations from unstructured visual data, yet existing approaches remain limited in their ability to harness in-the-wild images for scalable robot learning. For instance, previous *real-to-sim-to-real* methods [30, 41, 43, 52, 58] require explicit reconstruction of physical workspaces to build simulation environments for data generation. This reliance on scene-specific acquisition prevents them from leveraging arbitrary open-world images, fundamentally limiting their scalability. Meanwhile, recent works [6, 29, 63, 71, 76, 78] leverage vision generative models to predict future visual observations of robot actions within real-world scenes. However, due to the limitations of existing video generation models, they cannot provide explicit robot actions and struggle to generate long-horizon or instruction-driven tasks of higher complexity.

In this work, we introduce **IGen**, a novel framework that takes robotic data synthesis the extra mile by enabling scalable, diverse, and grounded visuomotor data generation from unannotated open-world images with minimal effort. It takes in-the-wild images as the sole visual input and leverages task and motion planning to automatically generate robot behaviors at scale without any human annotation. IGen further synthesizes large-scale visual observations and action trajectories that serve as high-quality training data for effective robot learning.

To be more specific, IGen employs the following unified pipeline to generate visuomotor data from open-world

images. First, rather than directly operating on unstructured 2D pixels, IGen leverages the strong visual capabilities of large vision models (LVM) to reconstruct scenes as 3D point clouds and spatial keypoints. Next, it utilizes the visual understanding capabilities of vision-language models (VLM) to perform high-level task planning in 3D pixel space and transform motions into low-level control functions. Meanwhile, to generate robot-environment interactions, IGen uses the end-effector $SE(3)$ trajectory to perform rigid-motion-based synthesis of the scene point cloud sequence. Finally, frame-wise rendering is applied to the entire point cloud sequence, generating action-consistent visual observations of the target manipulation task.

We evaluate IGen along three dimensions: (1) visual fidelity, measured by the consistency between the generated visual observations and real-world perception; (2) action quality, quantified by the scores of instruction following and physics alignment of the generated action videos; and (3) policy transferability, assessed through the performance of visuomotor policies trained on generated data and evaluated on real-world tasks. Experiments reveal that IGen generates visually realistic images and physically reliable robotic behaviors that align with specific task instructions, providing high-quality data for effective robot learning. Notably, results demonstrate that policies trained solely on IGen-generated data—without any human-annotated demonstrations—can outperform those trained on real-world trajectories.

In summary, our contributions are as follows:

- We propose an effective data generation framework that produces scalable visual-action datasets from open-world images, integrating cross-scene generalization, instruction diversity and long-horizon task applicability.
- We transform unstructured open-world images into actionable 3D scene representations that enable robotic task reasoning and motion planning, generating task-consistent behaviors aligned with the physical world. Furthermore, we introduce a simulation-free point cloud synthesis approach that produces realistic visual observations and supports large-scale robot experience generation.
- We demonstrate that robotic policies trained on IGen-generated data can successfully perform real-world manipulation tasks without any additional data collection. This suggests the promising potential of IGen to establish real-world images as an effective source for robot policy training, paving the way for scalable, annotation-free robot learning.

2. Related Work

2.1. Visuomotor Robot Learning

Recent progress in visuomotor policy learning [11, 19, 21, 68, 75, 77] enables robots to perform real-world manipulation tasks through end-to-end imitation learning from

paired visual and action demonstrations. Inspired by the development of large-scale vision–language models (VLM) [1, 3, 44], recent efforts have focused on scaling up model size and data volume to build more generalist robotic models [4, 5, 7, 24, 28, 33, 42, 55, 56]. Meanwhile, many studies [25, 26, 50] leverage the planning capabilities of VLMs to enable open-world robotic manipulation. Existing datasets [16, 18, 49, 57] have collected large-scale demonstration data across diverse real-world scenes and task settings. Meanwhile, recent works [10, 12, 14, 20, 32, 45, 62, 70, 72] focus on improving the efficiency and scalability of robotic data collection.

In contrast to vision–language models that benefit from abundant web-scale data, robotic learning lacks equivalent sources of large-scale, open-world demonstrations, posing a major bottleneck for developing generalist robot models [46]. Open-world internet images provide a vast and diverse source of scenes for improving the generalization of robot learning. The core objective of our work is to enable scalable generation of robot-relevant data from such unstructured visual sources.

2.2. Real-Sim-Real Data Generation

The Real-Sim-Real approach leverages real-world visual observations to build simulation workspaces for scalable policy learning and real-world transfer. Many recent works [13, 31, 40, 51, 59, 65, 80] employ digital twin or digital cousin approaches to recreate objects and spatial layouts for building simulation environments for robot training. However, such methods often struggle to capture fine-grained scene details for realistic world modeling. Meanwhile, some approaches [15, 30, 41, 43, 52, 58] leverage high-fidelity 3D reconstruction techniques to model real-world scenes from multi-view observations, which are instantiated as executable robot workspaces within simulation environments. These methods remain confined to task-specific environments and require extensive visual data collection for scene reconstruction.

Open-source internet images provide a rich and scalable data source that can cover most real-world scenarios. To leverage this advantage, RoLA [74] proposes an open-world, image-based framework for robot learning data generation. However, it relies on accurate physical property estimation for scene modeling and remains limited in modeling complex interactive manipulation tasks. IGen, on the other hand, leverages images as the primary data source without explicit physics-based reconstruction, offering a lightweight alternative to simulation-based pipelines.

2.3. Experience Synthesis from Unstructured Data

Inspired by the success of large-scale visual models, there is growing interest in leveraging vast amounts of unstructured internet data—such as images and videos—to pro-

vide scalable training sources for robot learning. Recent approaches [8, 9, 39, 54, 67, 79] synthesize robot manipulation data from collections of human demonstration videos from the Internet or real-world recordings. However, such data are limited in scene diversity and inherently suffer from human bias. Many works [29, 35, 63, 76, 78] build upon large-scale pre-trained video generation models to create visual observations for robotic manipulation. Yet, these generative methods often lack grounded robotic actions, struggle with complex and long-horizon tasks, and incur substantial computational costs. Images are the most abundant source of data on the internet, yet they inherently lack robot-relevant information. To this end, IGen aims to transform unstructured image data into grounded robotic experiences, providing a scalable source of data for robot learning.

3. Methodology

IGen is a robotic data generation framework that synthesizes task-specific robot actions and visual observations from open-world images. The architecture consists of three main stages: (1) **Scene Reconstruction**, converting the input image into a manipulable workspace for the robot; (2) **Action Planning**, reasoning over spatial keypoints to generate action trajectories; and (3) **Observation Synthesis**, composing and rendering point-cloud sequences to generate visual observations of the task.

3.1. From Pixels to Structured 3D Representations

Open-world images are unstructured and lack explicit robot-related actions. Hence, the key to enabling robotic learning from images lies in transforming raw pixels into structured representations that robots can effectively interpret and take actions upon. To this end, we adopt 3D point clouds as the modality, which offers a format better suited to visual observation and structured editing.

To begin with, we employ a versatile monocular geometric foundation model [23] to estimate the depth and geometric structure of the scene. Then, we employ Segment Anything Model [34] to obtain masks \mathcal{M} of task-relevant objects. Following the keypoints representation in [26], we extract scene features using DINOv2 [48]. Next, we apply K-means clustering to both the feature embeddings and 3D coordinates, resulting in a set of K spatial keypoints, denoted as $\mathcal{K} = \{k_j \in \mathbb{R}^3 \mid j = 1, 2, \dots, K\}$, with their associated 3D coordinates.

Then, the inpainting model [66] is applied to the original image to remove the target manipulable object and reconstruct the background image $\mathbf{I}_{\text{bg}} \in \mathbb{R}^{H \times W \times 3}$. Given the estimated depth map $\mathbf{D} \in \mathbb{R}^{H \times W}$ and the camera intrinsic matrix \mathbf{K} , all pixels are lifted into 3D space as a dense 3D point cloud $P_{\text{bg}} \in \mathbb{R}^{H \times W \times 6}$. To address incomplete modeling of manipulated objects from monocular views, we employ a 3D generative reconstruction model [61] to their

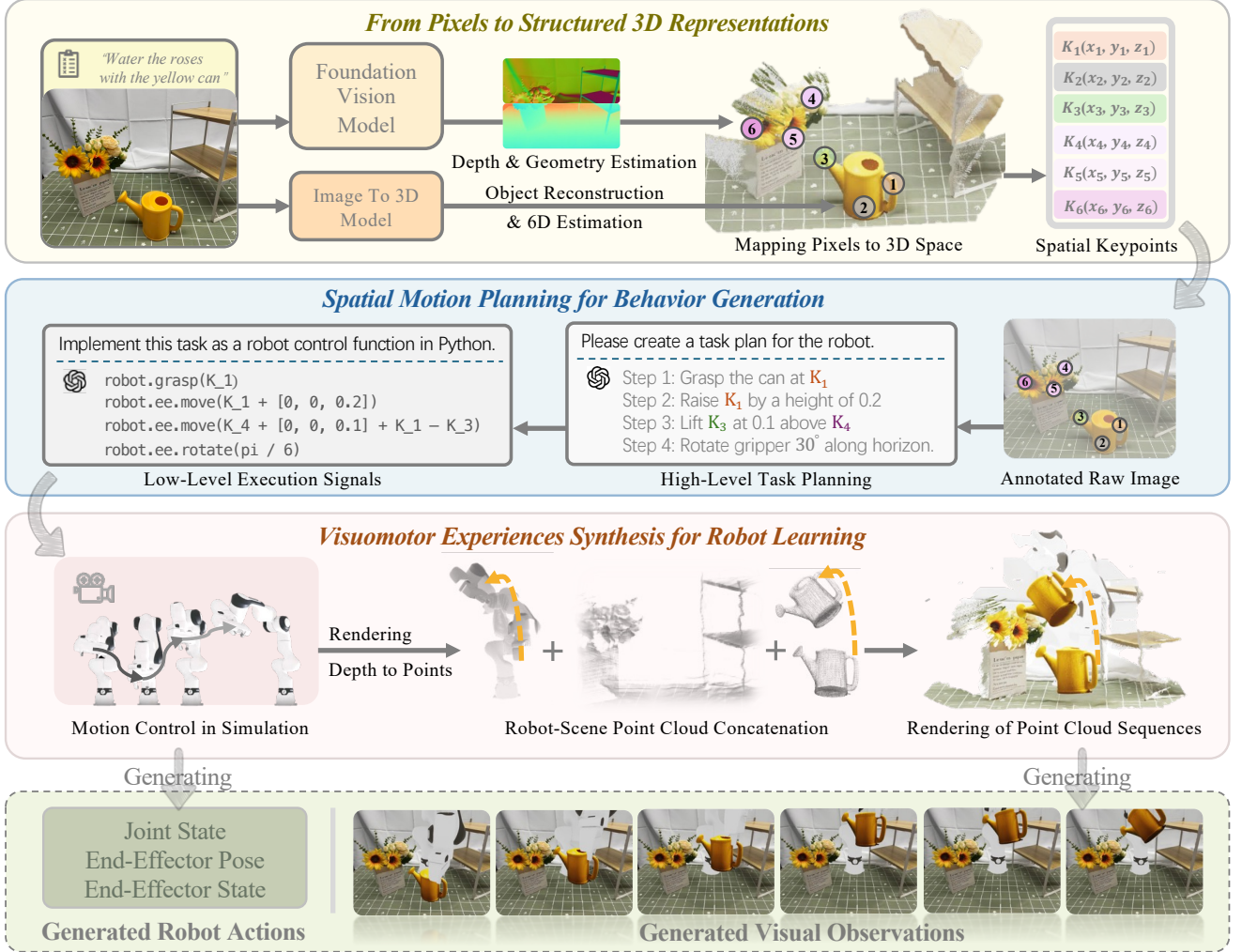


Figure 2. **Overview of IGen.** Given an open-world image and a task description, IGen first reconstructs the environment and objects as point clouds via Foundation Vision Models. After spatial keypoint extraction, VLM maps the task description to high-level plans and low-level control commands. During the robot’s execution in simulation, a virtual depth camera captures the motion point cloud sequences. The resulting end-effector pose trajectory is used to synthesize dynamic point-cloud sequences, which are then rendered frame-by-frame into visual observations of the manipulation. The final output consists of the generated robot actions and the visual observations.

full 3D shape and appearance. After reconstructing the objects into dense point clouds, we re-position the completed objects to their original pose using 6D pose estimation [38]. Furthermore, to enable spatial domain randomization, we extract a set of feasible placement points from the supporting surface (e.g., the spatial points of the tabletop), which serve as candidate spatial poses for object generalization. Details of the reconstruction are provided in the appendix.

3.2. Spatial Planning for Behavior Generation

Since open-world images lack action-related guidance for robots, we leverage the strong visual reasoning and planning capabilities of VLMs [1, 3] to guide robotic behavior generation. We provide the image annotated with keypoints

\mathcal{K} , their 3D coordinates, and the task instruction as inputs to the VLM. The VLM decomposes the overall task into a set of sub-stages $\mathcal{S} = \{S_i\}_{i=1}^N$ through high-level task planning. For each sub-stage, the VLM model generates an action description associated with the keypoints.

To enable robotic action execution, we develop an easily programmable control language in Python based on the end-effector’s $SE(3)$ pose, translating high-level task stages \mathcal{S} into executable low-level control functions $\mathcal{F} = \{f_i\}_{i=1}^N$ with VLM. For each task stage S_i , the function f_i is defined as a keypoint-conditioned solver that computes the reference end-effector pose from the spatial anchors in \mathcal{K}_i . During the pre-manipulation stage, the end-effector interacts precisely with the object based on a grasping prior model, where the



Figure 3. **Qualitative comparison of robotic behavior generation using IGen.** Given a single captured image and a natural-language manipulation instruction, Tesseract [76], Cosmos [2], and our IGen generate behavior observations. IGen produces more instruction-consistent and physically coherent object motions, closely matching the intended tasks. The green box represents action observations that adhere to physical laws and follow the task instructions, and the checkmark indicates task completion.

end-effector pose is predicted by the grasp model [17, 47], and the gripper state is determined by the point cloud width along the gripper’s principal axis. During manipulation, keypoints on the manipulated object are treated as movable points rigidly attached to the end-effector, while other keypoints serve as static scene anchors. The specific prompts used are detailed in the appendix.

Starting from the initial robot state x_0 , the motion planner produces a set of sub-goals $\mathcal{X} = \{\hat{x}_i\}_{i=1}^N$ that define the desired states for subsequent control execution. Each stage computes the next state as $\hat{x}_i = f_i(\hat{x}_{i-1})$, where $\hat{x}_0 = x_0$. We use a motion planner to generate feasible trajectories, which are then executed in a simulation environment, producing an action sequence $\mathcal{A} = \{a_t\}_{t=1}^T$ over T time steps, sampled at a fixed frame rate. Each action a_t includes the robot’s end-effector pose and joint positions. Detailed simulation settings are provided in the appendix.

3.3. Experience Synthesis for Robot Learning

To obtain visual observations synchronized with embodied actions, we propose a robotic experience synthesis framework based on real-time point cloud rendering. A complete

point cloud observation of a manipulation task comprises the action point cloud sequence of the robot and the dynamic point cloud sequence of the scene.

To synthesize action point clouds, the simulated robot is placed at the planned pose p_{robot} in simulation, and a virtual camera is positioned at p_{cam} , aligned with the viewpoint used for generating the scene point clouds. From the action sequence \mathcal{A} , we obtain an end-effector pose trajectory $\mathcal{T} = \{\mathbf{T}_t\}_{t=1}^T$, where $\mathbf{T}_t \in SE(3)$ denotes the 6-DoF pose of the end-effector at time step t , including both rotation and translation. At each time step t , the environment is rendered to produce synchronized RGB and depth frames, which are then back-projected through the virtual camera \mathbf{C} to construct the point cloud sequence of the robot’s motion $\mathcal{P}_{\text{robot}} = \{P_{\text{robot},t}\}_{t=1}^T$. Meanwhile, the background is modeled as a static point cloud sequence \mathcal{P}_{bg} .

We perform dynamic interaction between the end-effector and the point clouds based on transformations of the end-effector’s pose. Assume the grasp is established at time t_g , with the object’s pose $\mathbf{T}_{\text{obj},t_g}$ and the end-effector pose \mathbf{T}_{t_g} . For all time steps $t \in \mathcal{T}_{\text{grasp}}$, where $\mathcal{T}_{\text{grasp}}$ denotes the set of time indices during which the gripper remains closed on the

Task	PSNR \uparrow		SSIM \uparrow		FID \downarrow		LPIPS \downarrow		LPIPS \downarrow		LPIPS \downarrow	
	Real-to-Sim	IGen	Real-to-Sim	IGen	Real-to-Sim	IGen	Real-to-Sim	IGen	Real-to-Sim	IGen	Real-to-Sim	IGen
Pick Carrot on Plate	18.1480	28.2611	0.6756	0.8371	0.0001	0.0001	0.2864	0.0518	0.3882	0.1166	0.2057	0.0418
Put Eggplant in Basket	16.6910	23.2821	0.7706	0.8350	0.0001	0.0009	0.2458	0.0825	0.2658	0.1242	0.1682	0.0547
Put Spoon on Towel	15.9262	26.7524	0.6041	0.8621	0.0061	0.0008	0.4275	0.0621	0.4879	0.1129	0.2980	0.0433
Stack Cubes	18.2944	29.7206	0.6828	0.8747	0.0030	0.0003	0.3345	0.0558	0.4419	0.1021	0.2491	0.0386
Average	17.2649	27.0040	0.6833	0.8522	0.0023	0.0005	0.3235	0.0630	0.3959	0.1139	0.2302	0.0446

Table 1. We compare the visual similarity between the digital-twin scenes reconstructed by Real-to-Sim and those generated by IGen. Real-to-Sim refers to the method in Simpler [40] that converts real-world scenes into simulated digital-twin scenes. We compute the LPIPS [60] variants using AlexNet [36], VGGNet [53], and SqueezeNet [27], denoted as LPIPS₁, LPIPS₂, and LPIPS₃. \uparrow/\downarrow indicates higher/lower is better.

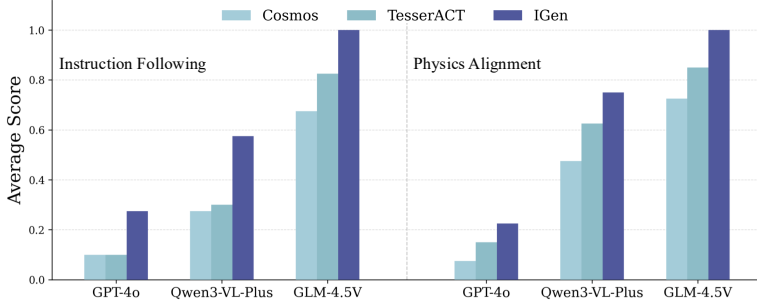


Figure 4. **Quantitative Comparison of robotic behavior generated by IGen.** Performance is assessed on DreamGen Bench [29] under two criteria: *Instruction Following* and *Physics Alignment*. Evaluations are conducted using GPT-4o [1], Qwen-3-VL-Plus [3] and GLM-4.5V [69] as video assessment models. Each method generates 40 videos along with the prompts, and the reported metric represents the proportion of videos receiving a score of 1 from the evaluator.

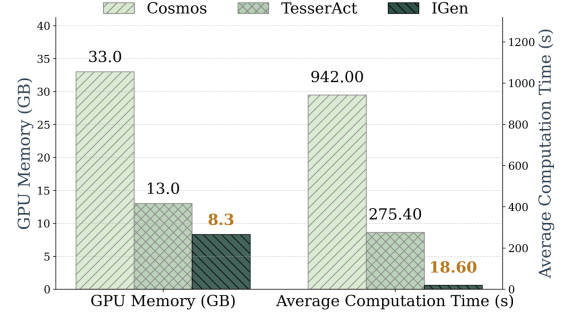


Figure 5. **Evaluation of IGen's computational efficiency.** We compare the video generation time and GPU memory consumption of IGen and baselines under identical input images and task instructions. The average computation time refers to the time required to generate one robot behavior video.

object, the world pose the object evolves by rigidly following the end-effector. The manipulated object, represented as a point cloud sequence $\mathcal{P}_{\text{obj}} = \{P_{\text{obj},t}\}_{t=1}^T$, undergoes rigid-body transformations induced by the end-effector poses. The transformation at time t can be expressed as:

$$P_{\text{obj},t} = \begin{cases} P_{\text{obj},t} & t \notin \mathcal{T}_{\text{grasp}}, \\ \mathbf{T}_t (\mathbf{T}_{t_g})^{-1} \mathbf{T}_{\text{obj},t_g} P_{\text{obj},t_g} & t \in \mathcal{T}_{\text{grasp}}. \end{cases} \quad (1)$$

By combining the static environment, the robot, and the manipulated object, we represent the complete task as a composite point cloud sequence:

$$\mathcal{P}_{\text{task}} = \mathcal{P}_{\text{bg}} \cup \mathcal{P}_{\text{obj}} \cup \mathcal{P}_{\text{robot}}. \quad (2)$$

By rendering the point cloud sequence through the virtual camera \mathbf{C} , we obtain the visual observations \mathcal{O} . The temporally synchronized observations, together with the action sequence \mathcal{A} , constitute the paired visual-action data for robot learning.

4. Experiment

In this section, we aim to address the following three research questions: (1) Can **IGen** generate visually realistic

data from real-world images across various scenes? (2) Can **IGen** efficiently generate robot actions that align with the environment and follow task instructions? (3) Can **IGen** synthesize effective robotic training data directly from a single image, enabling policy training and real-world deployment without any human-teleoperated demonstrations?

4.1. Scene Reconstruction Fidelity

In this section, we compare IGen with Real-to-Sim methods to measure the visual realism of the synthesized scenes. We conduct experiments on the Simpler dataset [40], which provides diverse real-world robotic manipulation scenes. Based on the real-world captured images in Simpler, we employ IGen to reconstruct the corresponding 3D scenes for evaluation. Meanwhile, the Real-to-Sim method in Simpler reconstructs digital-twin scenes from real-world images.

We adopt multiple visual metrics, including PSNR, SSIM, FID, and LPIPS [60], to assess the visual consistency between the original real-world scenes and those reconstructed by the Real-to-Sim method in Simpler or IGen.

As shown in Tab. 1, IGen achieves superior performance across multiple evaluation metrics. For instance, using LPIPS scores computed across multiple perception models to

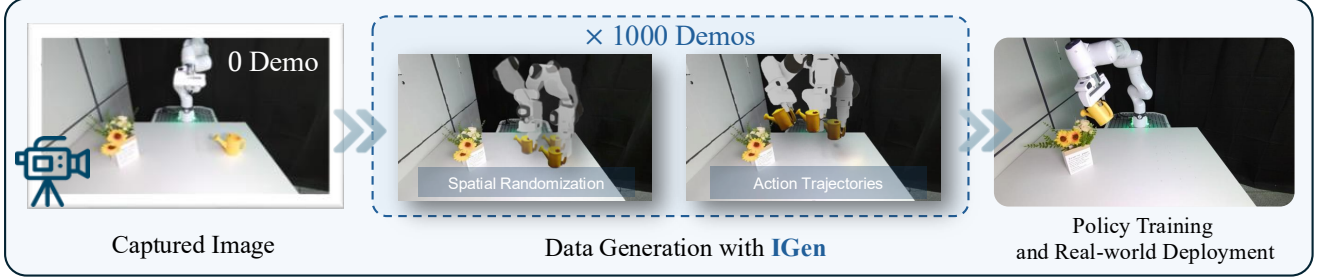


Figure 6. **Experimental setup.** Starting from a captured real-world scene image, IGen automatically generates 1,000 task demonstrations with spatial randomization. The resulting data are used to train a visuomotor policy, which is later deployed and evaluated in the real world.

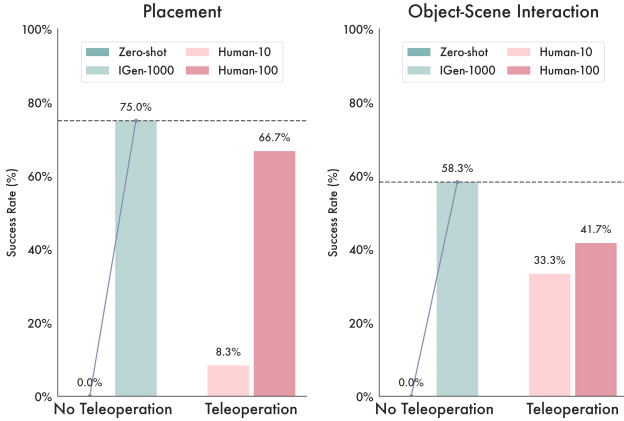


Figure 7. **Real-world robot evaluation results.** We assess policy performance on real-world tasks, comparing task success rates under four different conditions: zero-shot, fine-tuned with 10 human teleoperation data, fine-tuned with 100 human teleoperation data, and fine-tuned with 1,000 IGen-synthesized data.

assess the perceptual discrepancy between generated scenes and the original images, we observe that IGen achieves up to a $5.13\times$ improvement in similarity compared with the Real-to-Sim baseline. These results indicate that the scenes generated by IGen remain highly consistent with the corresponding real-world images, demonstrating its capability to produce visually faithful and realistic observations that align closely with real environments, thus mitigating the sim-to-real gap.

4.2. Evaluation of Behavior Generation

This section focuses on evaluating the behavioral accuracy and instruction alignment of the videos of robotic behaviors generated with IGen. We evaluate IGen across diverse visual sources and task instructions to assess the quality of robotic behaviors generated from a single image. For comparison, we include Cosmos-Predict2 [2, 29] and Tesseract [76] as baselines, both of which are capable of generating robot behaviors from a single image input. Cosmos-Predict2 employs the Cosmos-Predict2-2B-Video2World model, while

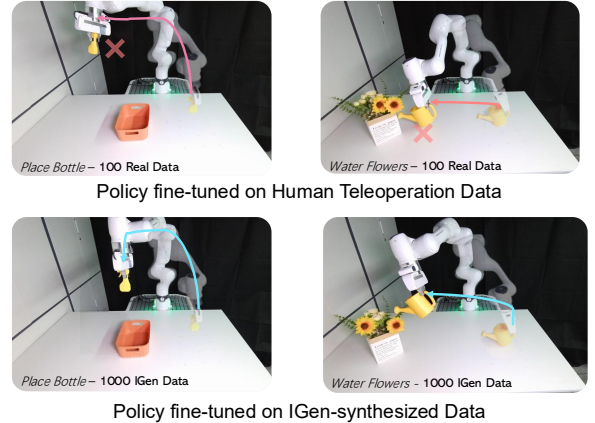


Figure 8. **Effectiveness of IGen for Robot Learning.** We demonstrate that policies trained on IGen-synthesized data outperform those trained on limited on-robot data. The blue trajectory represents actions that correctly follow the task instructions, while the red trajectory indicates deviations from the target action.

Tesseract uses the video generation model fine-tuned from CogVideoX-5B-I2V [64].

Qualitative Experiments. As shown in Fig. 3, we evaluate on unlabeled, open-world images without any task annotations or demonstrations. Each image is associated with a scene-specific instruction, which serves as a high-level command for IGen and as the language prompt for Cosmos-Predict2 and Tesseract. The results demonstrate that IGen can generate complete and coherent robotic behaviors that accurately follow the given task instructions, producing physically consistent motions and visual observations that align with real-world physics. In contrast, the baseline methods exhibit temporal discontinuities, geometric distortions, and inaccurate motion execution, failing to produce instruction-aligned behaviors.

Quantitative Experiments. To comprehensively evaluate the quality of robotic behaviors generated by IGen, we conduct experiments on the DreamGen Bench [29]. Two criteria—*Instruction Following* and *Physics Alignment*—

are used to assess the quality of the generated robot-manipulation videos. We employ GPT-4o [1], Qwen-3-VL-Plus [3], and GLM-4.5V [69] as evaluation models, ensuring fair and consistent comparison under identical video resolution and frame-rate settings. As shown in Fig. 4, IGen outperforms all compared models in both *Instruction Following* and *Physics Alignment*. As shown in the results, IGen produces nearly **twice** as many *Instruction Following* successes as the baseline when evaluated by Qwen-3-VL-Plus. Furthermore, under the *Physics Alignment* metric, GLM-4.5V judges **100%** of IGen-generated videos to exhibit physically consistent dynamics. These results indicate that IGen provides high-quality visual observations and physically accurate action sequences, which can effectively support robot learning in real-world environments.

Computational Efficiency. For large-scale model training, generating data at scale requires high computational efficiency. In this section, we evaluate IGen’s computational efficiency, focusing on the runtime performance and resource consumption. For open-world image inputs, we use IGen to generate 1,000 randomized samples per image and report the average per-sample generation time and GPU memory utilization. For comparison, we compute the average per-sample video generation time and GPU memory utilization for Cosmos-Predict2 and Tesseract. As illustrated in Fig. 5, IGen demonstrates higher efficiency in data generation, requiring only 8.3 GB of GPU memory and approximately 18.6 seconds per sample. Under the same GPU memory conditions, IGen achieves data generation with approximately **30×** and **200×** higher efficiency than Tesseract and Cosmos-Predict2, respectively. These results highlight that IGen is significantly more computationally efficient and scalable for large-scale robotic data synthesis.

4.3. Robot Learning from Unstructured Images

We provide IGen with a single image and, without any on-robot data, automatically generate visuomotor data to train the robot model for real-world manipulation tasks.

Hardware Setup. All real-world experiments are conducted on a Franka Research 3 robot arm. Perception is provided by a single Microsoft Kinect RGB-D camera mounted in front of the manipulator, from which we use only the RGB stream as visual input.

Robot Policy. We adopt π_0 [5] as the base vision-language-action model. We first verify that, without any fine-tuning, π_0 achieves an almost zero success rate across our tasks, indicating limited zero-shot transfer capability in our experimental setting. Subsequently, the model is fine-tuned separately on teleoperation data and on IGen-generated data with LoRA [22], and evaluated on the same set of manipulation tasks for comparison.

Tasks and Evaluation. We design diverse manipulation

tasks to evaluate the effectiveness of IGen, covering two types: Placement (“*Place the bottle*”), Scene-Object Interaction (“*Water the flowers*”). We assess the effect of data scaling by training the model with (a) 10 real-robot samples, (b) 100 real-robot samples, and (c) 1,000 IGen-generated samples, and evaluating them under the same conditions.

Data Generation. Starting from a single camera-view image, IGen applies spatial randomization to generate training data for real-world scenes. A manipulable tabletop workspace is designated within the robot’s reachable area, and 3D points within this region are randomly sampled from the scene point cloud as object placement positions. As shown in Fig. 6, we generate 1,000 data samples with spatial randomization for each task.

Performance Analysis. As shown in Fig. 7, when directly deploying the π_0 model without any fine-tuning samples, the success rate remains close to zero. With just a single image, IGen automatically generates 1,000 synthetic data samples for policy fine-tuning. On *Place Bottle* task, the fine-tuned model achieves a significant increase in task success rate, increasing **from 0.0% to 75.0%**. Notably, the policy trained on 1,000 IGen-generated data, **without any on-robot data fine-tuning**, surpasses the success rates of 8.3% with 10 on-robot data and 66.7% with 100 on-robot data. As shown in Fig. 8, the policy fine-tuned on a small amount of real data exhibits deviations in action trajectory execution. In contrast, the policy fine-tuned on a large scale of IGen-generated data demonstrates more robust performance in executing task trajectories. The result suggest that IGen can serve as an effective and scalable alternative to human teleoperation for training robot policies. These findings highlight the potential to enable robots to learn from a wide range of open-world images, further enhancing its applicability for diverse real-world tasks. More details are provided in the appendix.

5. Conclusion

In this work, we propose a novel data generation framework that transforms open-world images into high-quality visuomotor data for robot learning. Leveraging only unstructured open-world images, our approach enables the scalable generation of training data, eliminating the need for human effort while effectively improving robot policy performance. This work has the potential to alleviate the challenge of limited real-world robot data, offering a promising data-driven solution for the development of generalist robot policies.

Limitations. Our method relies on the capabilities of foundational vision models, and its performance may be limited in images with visual defects. We look forward to stronger foundational models bringing improvements in the future.

References

- [1] Josh Achiam, Steven Adler, Sandhini Agarwal, Lama Ahmad, Ilge Akkaya, Florencia Leoni Aleman, Diogo Almeida, Janko Altenschmidt, Sam Altman, Shyamal Anadkat, et al. Gpt-4 technical report. *arXiv preprint arXiv:2303.08774*, 2023. 2, 3, 4, 6, 8
- [2] Niket Agarwal, Arslan Ali, Maciej Bala, Yogesh Balaji, Erik Barker, Tiffany Cai, Prithvijit Chattopadhyay, Yongxin Chen, Yin Cui, Yifan Ding, et al. Cosmos world foundation model platform for physical ai. *arXiv preprint arXiv:2501.03575*, 2025. 5, 7
- [3] Shuai Bai, Keqin Chen, Xuejing Liu, Jialin Wang, Wenbin Ge, Sibao Song, Kai Dang, Peng Wang, Shijie Wang, Jun Tang, et al. Qwen2. 5-vl technical report. *arXiv preprint arXiv:2502.13923*, 2025. 2, 3, 4, 6, 8
- [4] Johan Bjorck, Fernando Castañeda, Nikita Cherniadev, Xingye Da, Runyu Ding, Linxi Fan, Yu Fang, Dieter Fox, Fengyuan Hu, Spencer Huang, et al. Gr00t n1: An open foundation model for generalist humanoid robots. *arXiv preprint arXiv:2503.14734*, 2025. 2, 3
- [5] Kevin Black, Noah Brown, Danny Driess, Adnan Esmail, Michael Equi, Chelsea Finn, Niccolo Fusai, Lachy Groom, Karol Hausman, Brian Ichter, et al. pi.0: A vision-language-action flow model for general robot control. *arXiv preprint arXiv:2410.24164*, 2024. 2, 3, 8
- [6] Jake Bruce, Michael D Dennis, Ashley Edwards, Jack Parker-Holder, Yuge Shi, Edward Hughes, Matthew Lai, Aditi Mavalankar, Richie Steigerwald, Chris Apps, et al. Genie: Generative interactive environments. In *Forty-first International Conference on Machine Learning*, 2024. 2
- [7] Hao Chen, Jiaming Liu, Chenyang Gu, Zhuoyang Liu, Renrui Zhang, Xiaoqi Li, Xiao He, Yandong Guo, Chi-Wing Fu, Shanghang Zhang, et al. Fast-in-slow: A dual-system foundation model unifying fast manipulation within slow reasoning. *arXiv preprint arXiv:2506.01953*, 2025. 3
- [8] Hanzhi Chen, Boyang Sun, Anran Zhang, Marc Pollefeys, and Stefan Leutenegger. Vidbot: Learning generalizable 3d actions from in-the-wild 2d human videos for zero-shot robotic manipulation. In *Proceedings of the Computer Vision and Pattern Recognition Conference*, pages 27661–27672, 2025. 3
- [9] Yuanpei Chen, Chen Wang, Yaodong Yang, and C Karen Liu. Object-centric dexterous manipulation from human motion data. *arXiv preprint arXiv:2411.04005*, 2024. 3
- [10] Xuxin Cheng, Jialong Li, Shiqi Yang, Ge Yang, and Xiaolong Wang. Open-television: Teleoperation with immersive active visual feedback. *arXiv preprint arXiv:2407.01512*, 2024. 3
- [11] Cheng Chi, Zhenjia Xu, Siyuan Feng, Eric Cousineau, Yilun Du, Benjamin Burchfiel, Russ Tedrake, and Shuran Song. Diffusion policy: Visuomotor policy learning via action diffusion. *The International Journal of Robotics Research*, page 02783649241273668, 2023. 2
- [12] Cheng Chi, Zhenjia Xu, Chuer Pan, Eric Cousineau, Benjamin Burchfiel, Siyuan Feng, Russ Tedrake, and Shuran Song. Universal manipulation interface: In-the-wild robot teaching without in-the-wild robots. *arXiv preprint arXiv:2402.10329*, 2024. 3
- [13] Tianyuan Dai, Josiah Wong, Yunfan Jiang, Chen Wang, Cem Gokmen, Ruohan Zhang, Jiajun Wu, and Li Fei-Fei. Automated creation of digital cousins for robust policy learning. *arXiv preprint arXiv:2410.07408*, 2024. 3
- [14] Runyu Ding, Yuzhe Qin, Jiyue Zhu, Chengzhe Jia, Shiqi Yang, Ruihan Yang, Xiaojuan Qi, and Xiaolong Wang. Bunny-visionpro: Real-time bimanual dexterous teleoperation for imitation learning. *arXiv preprint arXiv:2407.03162*, 2024. 3
- [15] Jiafei Duan, Yi Ru Wang, Mohit Shridhar, Dieter Fox, and Ranjay Krishna. Ar2-d2: Training a robot without a robot. *arXiv preprint arXiv:2306.13818*, 2023. 3
- [16] Frederik Ebert, Yanlai Yang, Karl Schmeckpeper, Bernadette Bucher, Georgios Georgakis, Kostas Daniilidis, Chelsea Finn, and Sergey Levine. Bridge data: Boosting generalization of robotic skills with cross-domain datasets. *arXiv preprint arXiv:2109.13396*, 2021. 3
- [17] Hao-Shu Fang, Chenxi Wang, Minghao Gou, and Cewu Lu. Graspnet-1billion: A large-scale benchmark for general object grasping. In *Proceedings of the IEEE/CVF conference on computer vision and pattern recognition*, pages 11444–11453, 2020. 5
- [18] Hao-Shu Fang, Hongjie Fang, Zhenyu Tang, Jirong Liu, Chenxi Wang, Junbo Wang, Haoyi Zhu, and Cewu Lu. Rh20t: A comprehensive robotic dataset for learning diverse skills in one-shot. *arXiv preprint arXiv:2307.00595*, 2023. 3
- [19] Zipeng Fu, Tony Z Zhao, and Chelsea Finn. Mobile aloha: Learning bimanual mobile manipulation with low-cost whole-body teleoperation. *arXiv preprint arXiv:2401.02117*, 2024. 2
- [20] Jensen Gao, Annie Xie, Ted Xiao, Chelsea Finn, and Dorsa Sadigh. Efficient data collection for robotic manipulation via compositional generalization. *arXiv preprint arXiv:2403.05110*, 2024. 3
- [21] Nicklas Hansen, Zhecheng Yuan, Yanjie Ze, Tongzhou Mu, Aravind Rajeswaran, Hao Su, Huazhe Xu, and Xiaolong Wang. On pre-training for visuo-motor control: Revisiting a learning-from-scratch baseline. *arXiv preprint arXiv:2212.05749*, 2022. 2
- [22] Edward J Hu, Yelong Shen, Phillip Wallis, Zeyuan Allen-Zhu, Yuanzhi Li, Shean Wang, Lu Wang, and Weizhu Chen. LoRA: Low-rank adaptation of large language models. In *International Conference on Learning Representations*, 2022. 8, 2
- [23] Mu Hu, Wei Yin, Chi Zhang, Zhipeng Cai, Xiaoxiao Long, Hao Chen, Kaixuan Wang, Gang Yu, Chunhua Shen, and Shaojie Shen. Metric3d v2: A versatile monocular geometric foundation model for zero-shot metric depth and surface normal estimation. *IEEE Transactions on Pattern Analysis and Machine Intelligence*, 2024. 3, 1
- [24] Huang Huang, Fangchen Liu, Letian Fu, Tingfan Wu, Mustafa Mukadam, Jitendra Malik, Ken Goldberg, and Pieter Abbeel. Otter: A vision-language-action model with text-aware visual feature extraction. *arXiv preprint arXiv:2503.03734*, 2025. 3
- [25] Wenlong Huang, Chen Wang, Ruohan Zhang, Yunzhu Li, Jiajun Wu, and Li Fei-Fei. Voxposer: Composable 3d value maps for robotic manipulation with language models. *arXiv preprint arXiv:2307.05973*, 2023. 3

- [26] Wenlong Huang, Chen Wang, Yunzhu Li, Ruohan Zhang, and Li Fei-Fei. Rekep: Spatio-temporal reasoning of relational keypoint constraints for robotic manipulation. *arXiv preprint arXiv:2409.01652*, 2024. 3
- [27] Forrest N Iandola, Song Han, Matthew W Moskewicz, Khalid Ashraf, William J Dally, and Kurt Keutzer. Squeezenet: Alexnet-level accuracy with 50x fewer parameters and 0.5 mb model size. *arXiv preprint arXiv:1602.07360*, 2016. 6
- [28] Physical Intelligence, Kevin Black, Noah Brown, James Darpinian, Karan Dhabalia, Danny Driess, Adnan Esmail, Michael Equi, Chelsea Finn, Niccolo Fusai, et al. pi.0.5: a vision-language-action model with open-world generalization. *arXiv preprint arXiv:2504.16054*, 2025. 3
- [29] Joel Jang, Seonghyeon Ye, Zongyu Lin, Jiannan Xiang, Johan Bjorck, Yu Fang, Fengyuan Hu, Spencer Huang, Kaushil Kundalia, Yen-Chen Lin, et al. Dreamgen: Unlocking generalization in robot learning through neural trajectories. *arXiv e-prints*, pages arXiv–2505, 2025. 2, 3, 6, 7
- [30] Yufei Jia, Guangyu Wang, Yuhang Dong, Junzhe Wu, Yypei Zeng, Haonan Lin, Zifan Wang, Haizhou Ge, Weibin Gu, Kairui Ding, et al. Discoverse: Efficient robot simulation in complex high-fidelity environments. *arXiv preprint arXiv:2507.21981*, 2025. 2, 3
- [31] Zhenyu Jiang, Cheng-Chun Hsu, and Yuke Zhu. Ditto: Building digital twins of articulated objects from interaction. In *Proceedings of the IEEE/CVF Conference on Computer Vision and Pattern Recognition*, pages 5616–5626, 2022. 3
- [32] Zhenyu Jiang, Yuqi Xie, Kevin Lin, Zhenjia Xu, Weikang Wan, Ajay Mandlekar, Linxi Jim Fan, and Yuke Zhu. Dexmimicgen: Automated data generation for bimanual dexterous manipulation via imitation learning. In *2025 IEEE International Conference on Robotics and Automation (ICRA)*, pages 16923–16930. IEEE, 2025. 3
- [33] Moo Jin Kim, Karl Pertsch, Siddharth Karamcheti, Ted Xiao, Ashwin Balakrishna, Suraj Nair, Rafael Rafailov, Ethan Foster, Grace Lam, Pannag Sanketi, et al. Openvla: An open-source vision-language-action model. *arXiv preprint arXiv:2406.09246*, 2024. 2, 3
- [34] Alexander Kirillov, Eric Mintun, Nikhila Ravi, Hanzi Mao, Chloe Rolland, Laura Gustafson, Tete Xiao, Spencer Whitehead, Alexander C Berg, Wan-Yen Lo, et al. Segment anything. In *Proceedings of the IEEE/CVF international conference on computer vision*, pages 4015–4026, 2023. 3, 1
- [35] Po-Chen Ko, Jiayuan Mao, Yilun Du, Shao-Hua Sun, and Joshua B Tenenbaum. Learning to act from actionless videos through dense correspondences. *arXiv preprint arXiv:2310.08576*, 2023. 3
- [36] Alex Krizhevsky, Ilya Sutskever, and Geoffrey E Hinton. Imagenet classification with deep convolutional neural networks. *Advances in neural information processing systems*, 25, 2012. 6
- [37] Hugo Laurençon, Léo Tronchon, Matthieu Cord, and Victor Sanh. What matters when building vision-language models? *Advances in Neural Information Processing Systems*, 37: 87874–87907, 2024. 2
- [38] Taeyeop Lee, Bowen Wen, Minjun Kang, Gyuree Kang, In So Kweon, and Kuk-Jin Yoon. Any6d: Model-free 6d pose estimation of novel objects. In *Proceedings of the Computer Vision and Pattern Recognition Conference*, pages 11633–11643, 2025. 4
- [39] Marion Lepert, Jiaying Fang, and Jeannette Bohg. Phantom: Training robots without robots using only human videos. *arXiv preprint arXiv:2503.00779*, 2025. 3
- [40] Xuanlin Li, Kyle Hsu, Jiayuan Gu, Karl Pertsch, Oier Mees, Homer Rich Walke, Chuyuan Fu, Ishikaa Lunawat, Isabel Sieh, Sean Kirmani, et al. Evaluating real-world robot manipulation policies in simulation. *arXiv preprint arXiv:2405.05941*, 2024. 3, 6
- [41] Xinhai Li, Jialin Li, Ziheng Zhang, Rui Zhang, Fan Jia, Tiancai Wang, Haoqiang Fan, Kuo-Kun Tseng, and Ruiping Wang. Robogsim: A real2sim2real robotic gaussian splatting simulator. *arXiv preprint arXiv:2411.11839*, 2024. 2, 3
- [42] Jiaming Liu, Hao Chen, Pengju An, Zhuoyang Liu, Renrui Zhang, Chenyang Gu, Xiaoqi Li, Ziyu Guo, Sixiang Chen, Mengzhen Liu, et al. Hybridvla: Collaborative diffusion and autoregression in a unified vision-language-action model. *arXiv preprint arXiv:2503.10631*, 2025. 3
- [43] Haozhe Lou, Yurong Liu, Yike Pan, Yiran Geng, Jianteng Chen, Wenlong Ma, Chenglong Li, Lin Wang, Hengzhen Feng, Lu Shi, et al. Robo-gs: A physics consistent spatial-temporal model for robotic arm with hybrid representation. In *2025 IEEE International Conference on Robotics and Automation (ICRA)*, pages 15379–15386. IEEE, 2025. 2, 3
- [44] Haoyu Lu, Wen Liu, Bo Zhang, Bingxuan Wang, Kai Dong, Bo Liu, Jingxiang Sun, Tongzheng Ren, Zhuoshu Li, Hao Yang, et al. Deepseek-vl: towards real-world vision-language understanding. *arXiv preprint arXiv:2403.05525*, 2024. 2, 3
- [45] Ajay Mandlekar, Soroush Nasiriany, Bowen Wen, Iretiayo Akinola, Yashraj Narang, Linxi Fan, Yuke Zhu, and Dieter Fox. Mimicgen: A data generation system for scalable robot learning using human demonstrations. *arXiv preprint arXiv:2310.17596*, 2023. 3
- [46] Suvir Mirchandani, Suneel Belkhale, Joey Hejna, Evelyn Choi, Md Sazzad Islam, and Dorsa Sadigh. So you think you can scale up autonomous robot data collection? *arXiv preprint arXiv:2411.01813*, 2024. 2, 3
- [47] Adithyavairavan Murali, Balakumar Sundaralingam, Yu-Wei Chao, Wentao Yuan, Jun Yamada, Mark Carlson, Fabio Ramos, Stan Birchfield, Dieter Fox, and Clemens Eppner. Graspgen: A diffusion-based framework for 6-dof grasping with on-generator training. *arXiv preprint arXiv:2507.13097*, 2025. 5, 1
- [48] Maxime Oquab, Timothée Darcet, Théo Moutakanni, Huy Vo, Marc Szafraniec, Vasil Khalidov, Pierre Fernandez, Daniel Haziza, Francisco Massa, Alaaeldin El-Nouby, et al. Dinov2: Learning robust visual features without supervision. *arXiv preprint arXiv:2304.07193*, 2023. 3
- [49] Abby O'Neill, Abdul Rehman, Abhiram Maddukuri, Abhishek Gupta, Abhishek Padalkar, Abraham Lee, Acorn Pooley, Agrim Gupta, Ajay Mandlekar, Ajinkya Jain, et al. Open x-embodiment: Robotic learning datasets and rt-x models: Open x-embodiment collaboration 0. In *2024 IEEE International Conference on Robotics and Automation (ICRA)*, pages 6892–6903. IEEE, 2024. 3

- [50] Mingjie Pan, Jiyao Zhang, Tianshu Wu, Yinghao Zhao, Wenlong Gao, and Hao Dong. Omnimanip: Towards general robotic manipulation via object-centric interaction primitives as spatial constraints. In *Proceedings of the Computer Vision and Pattern Recognition Conference*, pages 17359–17369, 2025. 3
- [51] Shivansh Patel, Xinchun Yin, Wenlong Huang, Shubham Garg, Hooshang Nayyeri, Li Fei-Fei, Svetlana Lazebnik, and Yunzhu Li. A real-to-sim-to-real approach to robotic manipulation with vlm-generated iterative keypoint rewards. *arXiv preprint arXiv:2502.08643*, 2025. 3
- [52] M Nomaan Qureshi, Sparsh Garg, Francisco Yandun, David Held, George Kantor, and Abhishek Silwal. SplatSim: Zero-shot sim2real transfer of rgb manipulation policies using gaussian splatting. In *2025 IEEE International Conference on Robotics and Automation (ICRA)*, pages 6502–6509. IEEE, 2025. 2, 3
- [53] Karen Simonyan and Andrew Zisserman. Very deep convolutional networks for large-scale image recognition. *arXiv preprint arXiv:1409.1556*, 2014. 6
- [54] Himanshu Gaurav Singh, Antonio Loquercio, Carmelo Sferazza, Jane Wu, Haozhi Qi, Pieter Abbeel, and Jitendra Malik. Hand-object interaction pretraining from videos. In *2025 IEEE International Conference on Robotics and Automation (ICRA)*, pages 3352–3360. IEEE, 2025. 3
- [55] Gemini Robotics Team, Saminda Abeyruwan, Joshua Ainslie, Jean-Baptiste Alayrac, Montserrat Gonzalez Arenas, Travis Armstrong, Ashwin Balakrishna, Robert Baruch, Maria Bauza, Michiel Blokzijl, et al. Gemini robotics: Bringing ai into the physical world. *arXiv preprint arXiv:2503.20020*, 2025. 3
- [56] Octo Model Team, Dibya Ghosh, Homer Walke, Karl Pertsch, Kevin Black, Oier Mees, Sudeep Dasari, Joey Hejna, Tobias Kreiman, Charles Xu, et al. Octo: An open-source generalist robot policy. *arXiv preprint arXiv:2405.12213*, 2024. 3
- [57] Zachary Teed and Jia Deng. Droid-slam: Deep visual slam for monocular, stereo, and rgb-d cameras. *Advances in neural information processing systems*, 34:16558–16569, 2021. 3
- [58] Marcel Torne, Arhan Jain, Jiayi Yuan, Vidaaranya Macha, Lars Ankile, Anthony Simeonov, Pulkit Agrawal, and Abhishek Gupta. Robot learning with super-linear scaling. *arXiv preprint arXiv:2412.01770*, 2024. 2, 3
- [59] Lirui Wang, Yiyang Ling, Zhecheng Yuan, Mohit Shridhar, Chen Bao, Yuzhe Qin, Bailin Wang, Huazhe Xu, and Xiaolong Wang. Gensim: Generating robotic simulation tasks via large language models. *arXiv preprint arXiv:2310.01361*, 2023. 3
- [60] Eugene P Wigner et al. The unreasonable effectiveness of mathematics in the natural sciences. *Mathematics and science*, 13:1–14, 1990. 6
- [61] Jianfeng Xiang, Zelong Lv, Sicheng Xu, Yu Deng, Ruicheng Wang, Bowen Zhang, Dong Chen, Xin Tong, and Jiaolong Yang. Structured 3d latents for scalable and versatile 3d generation. In *Proceedings of the Computer Vision and Pattern Recognition Conference*, pages 21469–21480, 2025. 3, 1
- [62] Zhengrong Xue, Shuying Deng, Zhenyang Chen, Yixuan Wang, Zhecheng Yuan, and Huazhe Xu. Demogen: Synthetic demonstration generation for data-efficient visuomotor policy learning. *arXiv preprint arXiv:2502.16932*, 2025. 3
- [63] Mengjiao Yang, Yilun Du, Kamyar Ghasemipour, Jonathan Tompson, Dale Schuurmans, and Pieter Abbeel. Learning interactive real-world simulators. *arXiv preprint arXiv:2310.06114*, 1(2):6, 2023. 2, 3
- [64] Zhuoyi Yang, Jiayan Teng, Wendi Zheng, Ming Ding, Shiyu Huang, Jiazhen Xu, Yuanming Yang, Wenyi Hong, Xiaohan Zhang, Guanyu Feng, et al. Cogvideox: Text-to-video diffusion models with an expert transformer. *arXiv preprint arXiv:2408.06072*, 2024. 7
- [65] Weirui Ye, Fangchen Liu, Zheng Ding, Yang Gao, Oleh Rybkin, and Pieter Abbeel. Video2policy: Scaling up manipulation tasks in simulation through internet videos. *arXiv preprint arXiv:2502.09886*, 2025. 3
- [66] Tao Yu, Runseng Feng, Ruoyu Feng, Jinming Liu, Xin Jin, Wenjun Zeng, and Zhibo Chen. Inpaint anything: Segment anything meets image inpainting. *arXiv preprint arXiv:2304.06790*, 2023. 3
- [67] Zhecheng Yuan, Tianming Wei, Langzhe Gu, Pu Hua, Tianhai Liang, Yuanpei Chen, and Huazhe Xu. Hermes: Human-to-robot embodied learning from multi-source motion data for mobile dexterous manipulation. *arXiv preprint arXiv:2508.20085*, 2025. 3
- [68] Yanjie Ze, Gu Zhang, Kangning Zhang, Chenyuan Hu, Muhan Wang, and Huazhe Xu. 3d diffusion policy: Generalizable visuomotor policy learning via simple 3d representations. *arXiv preprint arXiv:2403.03954*, 2024. 2
- [69] Aohan Zeng, Xin Lv, Qinkai Zheng, Zhenyu Hou, Bin Chen, Chengxing Xie, Cunxiang Wang, Da Yin, Hao Zeng, Jiajie Zhang, et al. GLM-4.5: Agentic, reasoning, and coding (arc) foundation models. *arXiv preprint arXiv:2508.06471*, 2025. 6, 8
- [70] Qiyuan Zeng, Chengmeng Li, Jude St John, Zhongyi Zhou, Junjie Wen, Guorui Feng, Yichen Zhu, and Yi Xu. Activeumi: Robotic manipulation with active perception from robot-free human demonstrations. *arXiv preprint arXiv:2510.01607*, 2025. 3
- [71] Hongxin Zhang, Zeyuan Wang, Qiushi Lyu, Zheyuan Zhang, Sunli Chen, Tianmin Shu, Behzad Dariush, Kwongjoon Lee, Yilun Du, and Chuang Gan. Combo: compositional world models for embodied multi-agent cooperation. *arXiv preprint arXiv:2404.10775*, 2024. 2
- [72] Han Zhang, Songbo Hu, Zhecheng Yuan, and Huazhe Xu. Doglove: Dexterous manipulation with a low-cost open-source haptic force feedback glove. *arXiv preprint arXiv:2502.07730*, 2025. 3
- [73] Jingyi Zhang, Jiaxing Huang, Sheng Jin, and Shijian Lu. Vision-language models for vision tasks: A survey. *IEEE transactions on pattern analysis and machine intelligence*, 46(8):5625–5644, 2024. 2
- [74] Siheng Zhao, Jiageng Mao, Wei Chow, Zeyu Shangguan, Tianheng Shi, Rong Xue, Yuxi Zheng, Yijia Weng, Yang You, Daniel Seita, et al. Robot learning from any images. In *Conference on Robot Learning*, pages 4226–4245. PMLR, 2025. 3

- [75] Tony Z Zhao, Vikash Kumar, Sergey Levine, and Chelsea Finn. Learning fine-grained bimanual manipulation with low-cost hardware. *arXiv preprint arXiv:2304.13705*, 2023. [2](#)
- [76] Haoyu Zhen, Qiao Sun, Hongxin Zhang, Junyan Li, Siyuan Zhou, Yilun Du, and Chuang Gan. Tesseract: learning 4d embodied world models. *arXiv preprint arXiv:2504.20995*, 2025. [2](#), [3](#), [5](#), [7](#)
- [77] Ray Chen Zheng, Kaizhe Hu, Zhecheng Yuan, Boyuan Chen, and Huazhe Xu. Extraneousness-aware imitation learning. *arXiv preprint arXiv:2210.01379*, 2022. [2](#)
- [78] Siyuan Zhou, Yilun Du, Jiaben Chen, Yandong Li, Dit-Yan Yeung, and Chuang Gan. Robodreamer: Learning compositional world models for robot imagination. *arXiv preprint arXiv:2404.12377*, 2024. [2](#), [3](#)
- [79] Junzhe Zhu, Yuanchen Ju, Junyi Zhang, Muhan Wang, Zhecheng Yuan, Kaizhe Hu, and Huazhe Xu. Dense-matcher: Learning 3d semantic correspondence for category-level manipulation from a single demo. *arXiv preprint arXiv:2412.05268*, 2024. [3](#)
- [80] Alex Zook, Fan-Yun Sun, Josef Spjut, Valts Blukis, Stan Birchfield, and Jonathan Tremblay. Grs: Generating robotic simulation tasks from real-world images. In *Proceedings of the Computer Vision and Pattern Recognition Conference*, pages 594–603, 2025. [3](#)

Appendix

A. Single-Image Scene Reconstruction Details

In this section, we describe how IGen reconstructs the 3D scene from a single open-world RGB image to facilitate robot data generation, as illustrated in Fig. 9.

We use Metric3Dv2 [23] to estimate the depth and convert image pixels into a point cloud. For open-world images, the focal length is fixed to 1000, while for specific camera types (e.g., iPhone or Microsoft Kinect Camera), we adopt their corresponding intrinsic parameters. The resulting point cloud preserves the same spatial resolution and dimensions as the original RGB image.

For object-level reconstruction, we utilize the TRELLIS model [61] to perform monocular 3D reconstruction and convert the outputs into colored point clouds. The input images to TRELLIS are pre-processed using segmentation masks obtained from SAM [34], ensuring that the reconstruction focuses on the target objects.

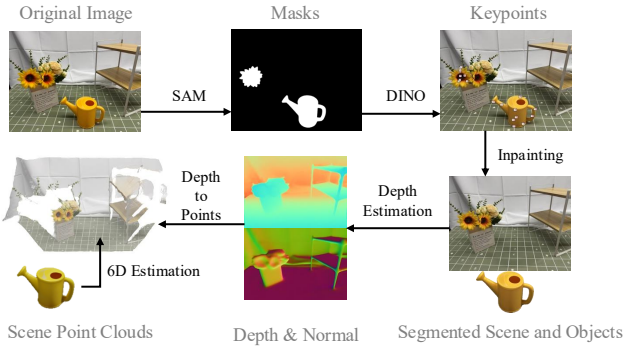


Figure 9. Single-Image Scene Reconstruction Pipeline.

B. Simulation Environment Details

This section describes the details of building the robotic manipulation platform in simulation. We adopt Isaac Sim as the simulation environment and deploy both the Franka Emika Panda and Franka Research 3 robotic arms within it. For motion planning, we utilize Curobo as the solver, which computes feasible trajectories given the target end-effector poses. We use the default illumination settings in the simulation environment.

As shown in Fig. 10, we place a virtual depth camera at the origin $[0, 0, 0]$ of the simulation scene, oriented relative to the robot’s base frame. The camera’s focal length is set to match that used in the depth estimation module. The robotic arm is positioned at a predefined spatial coordinate $[x_r, y_r, z_r]$ within the reconstructed point cloud space. During robot motion, the camera operates at a sampling rate of 30 fps, capturing synchronized RGB and depth frames

for subsequent reconstruction of the robot’s dynamic point cloud sequences.

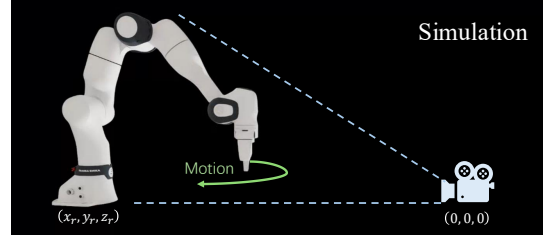


Figure 10. **Robot and Camera Placement in Simulation.** In simulation platforms such as IsaacSim, the virtual camera is placed at the position $(0, 0, 0)$, while the robotic arm base is positioned at the corresponding point in the point cloud, denoted as (x_r, y_r, z_r) . RGB and depth data are collected during the robotic arm’s motion.

C. Manipulation Synthesis Details

We divide the point cloud sequence into three components: the background point cloud, the robot point cloud, and the object point cloud. Among them, the robot and object point clouds are dynamic, while the background point cloud remains static. We use GraspGen [47] for grasp pose estimation.

The grasp width is inferred from the inter-point distance along the principal axis of the reconstructed object point cloud. At the grasping moment t_g , the end-effector pose is denoted as \mathbf{T}_{t_g} and the object pose as $\mathbf{T}_{\text{obj},t_g}$. During the subsequent manipulation at time t , given the current end-effector pose \mathbf{T}_t , the object pose in the scene can be computed through rigid-body transformation as:

$$\mathbf{T}_{\text{obj},t} = \mathbf{T}_t \mathbf{T}_{t_g}^{-1} \mathbf{T}_{\text{obj},t_g}. \quad (3)$$

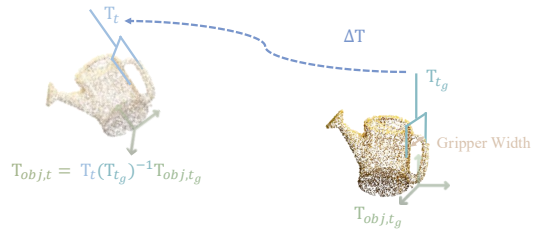


Figure 11. **Point Cloud Synthesis during Manipulation.** At time t_g , the object is grasped. The gripper width is calculated based on the point cloud, and the transformation of the object point cloud at time t is computed according to the end-effector’s pose.

D. Real-World Experiment Details

Hardware Setup. As shown in Fig. 12, we set up a real-world evaluation environment using the Franka Research 3 robotic arm. A Microsoft Kinect camera is placed in front of the robot to provide RGB visual input. The robotic arm performs task operations on the tabletop.

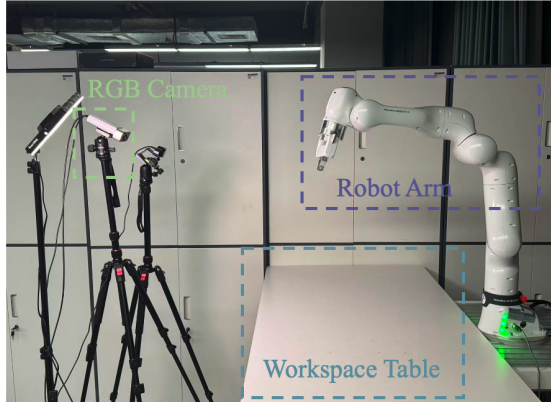


Figure 12. **Hardware Setup.** Our experimental setup consists of a Franka Research 3 robotic arm, a tabletop workspace, and a global RGB camera.

Spatial Randomization. For real-world data collection, we sample random object positions within a $40\text{ cm} \times 30\text{ cm}$ tabletop grid. In IGen, spatial randomization is performed based on the point cloud of the placement area (e.g., the tabletop surface). We define a 200×150 pixel grid as the sampling region for randomization, ensuring that the spatial distribution closely matches that of the real-world setup. Regarding the spatial randomization of real-world data and IGen-generated data, see Fig. 13 and 15.

Task Evaluation. We design diverse manipulation tasks involving complex interactions between objects and the surrounding scene. For each task, we conduct 12 independent trials. Object initial positions are sampled on a $30\text{ cm} \times 25\text{ cm}$ tabletop grid, with a spacing of 7 cm between adjacent positions. All models are evaluated using the same set of initial object positions.

Policy Learning. This section describes the fine-tuning process of policy. We fine-tune π_0 -base [5] for 30k training steps using LoRA [22] with a batch size of 8. The model takes as input a single 224×224 RGB image and the absolute joint positions as the state, and predicts a 10-step relative joint angle action chunk. Training is conducted on a single NVIDIA A40 GPU, requiring approximately 10.8 hours per training. The performance of the model in real-world deployment is shown in Fig. 16 and 17.

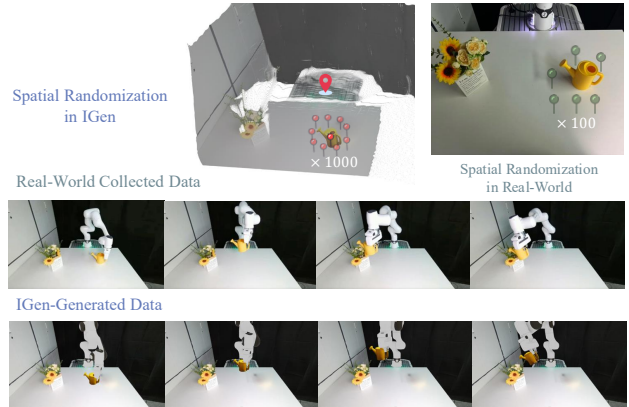


Figure 13. Spatial randomization of real-world data and IGen-generated data. The task is *Grab the watering can and water the flowers*.

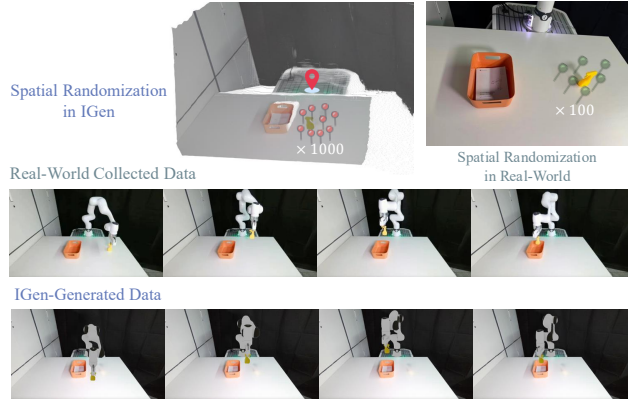


Figure 14. Spatial randomization of real-world data and IGen-generated data. The task is *Pick up the bottle and place it into the basket*.

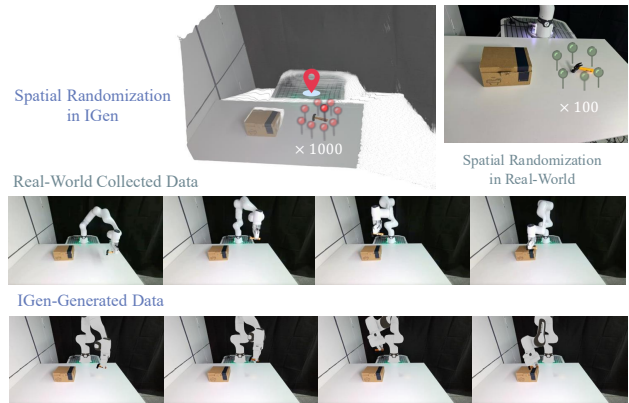


Figure 15. Spatial randomization of real-world data and IGen-generated data. The task is *Use the hammer to hit the cardboard box*.

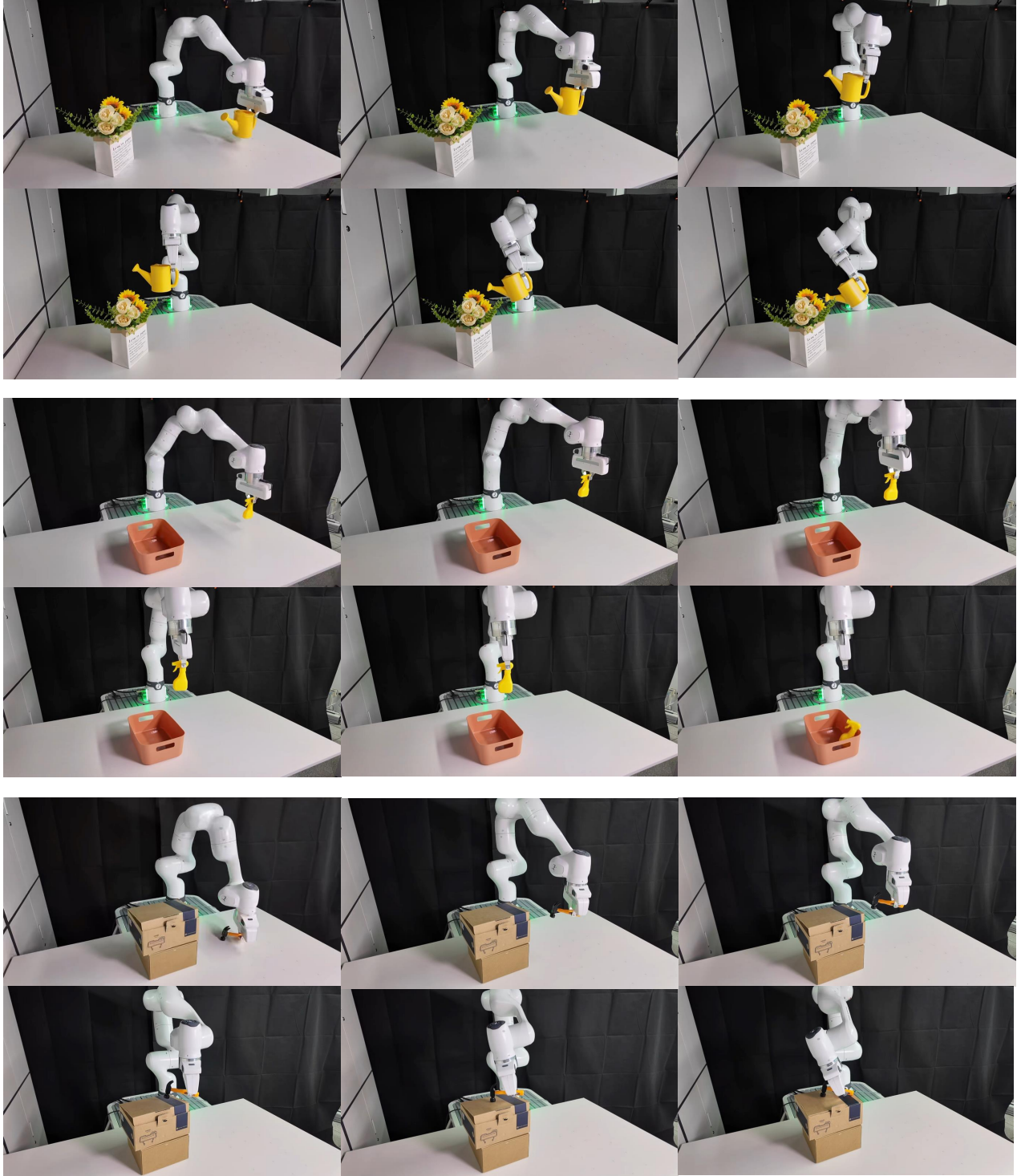


Figure 16. **Real-World Deployment of Policy trained with IGen-Generated Data.** The task instructions are as follows: *Grab the watering can and water the flowers. Pick up the bottle and place it into the basket. Use the hammer to hit the cardboard box.*

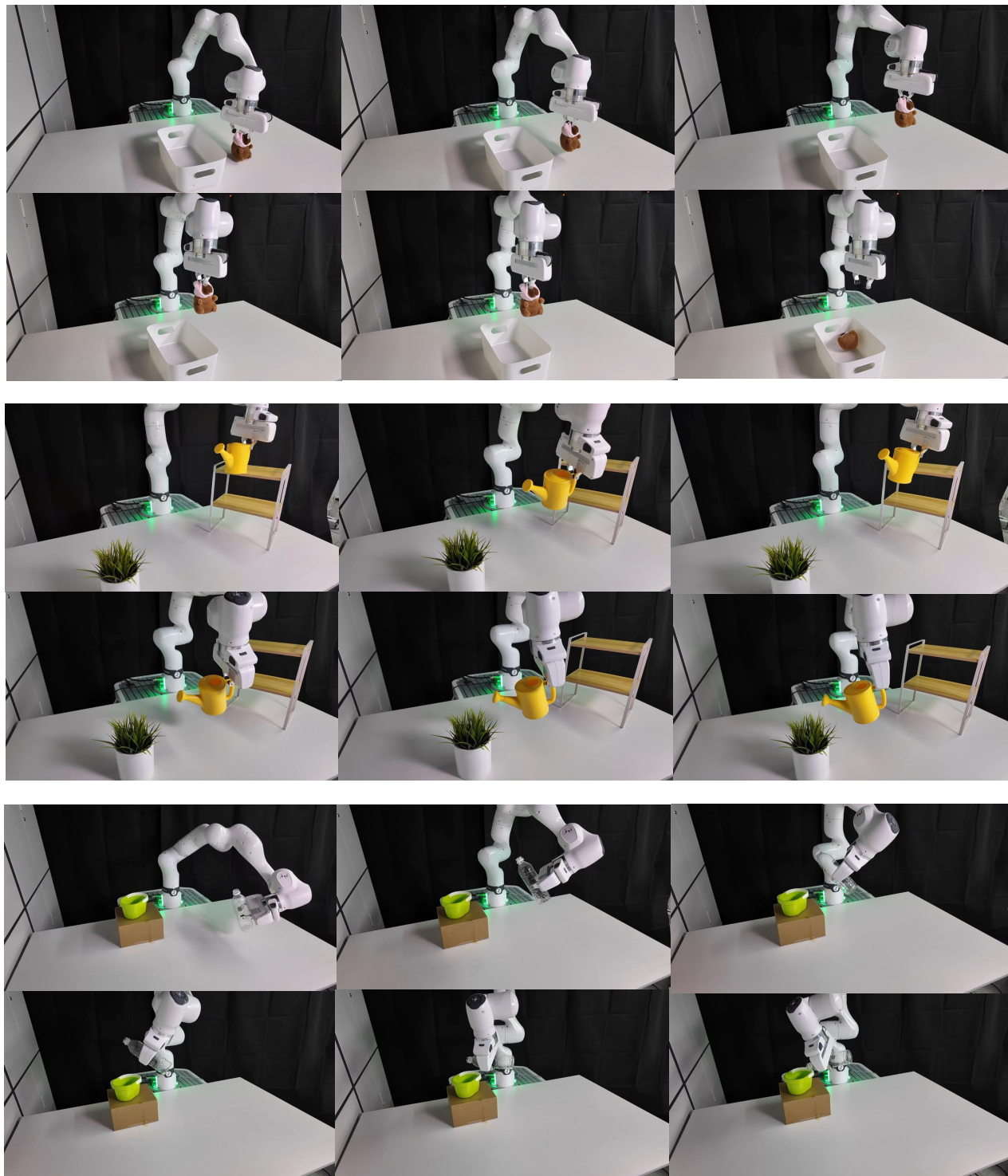


Figure 17. **Real-World Deployment of Policy trained with IGen-Generated Data.** The task instructions are as follows: *Grasp the toy and put it into the bin. Use the watering can on the cabinet to water the flowers. Pour water from the plastic bottle into the container.*